scientific reports

Check for updates

OPEN

Characterizing SSTR2 expression and modulation for targeted imaging and therapy in preclinical models of triple-negative breast cancer

Shannon E. Lynch[1,2], Corinne I. Crawford[1,5], Hailey A. Houson[1], James M. Omweri[3], Piyasuda Pukkanasut[3], Carlos A. Gallegos[1,5], Jason D. Whitt[4], Renata Jaskula-Sztul[4,6], Suzanne E. Lapi[1,3,6] & Anna G. Sorace[1,5,6]✉

Patients with breast cancer which lack molecular targets, such as human epidermal growth factor receptor 2 (HER2) or hormone receptors, have limited access to targeted therapies. Somatostatin receptor 2 (SSTR2) is overexpressed in some cancers, and SSTR2-targeted radiopharmaceuticals are FDA-approved for theranostic targeted imaging and therapy in neuroendocrine tumors (NETs). Importantly, histone deacetylase (HDAC) inhibitors can epigenetically modulate SSTR2 expression in NETs with low or variable basal expression. The goal of this study is to characterize SSTR2 basal expression and induction via HDAC inhibition as a potential target for imaging and therapy in preclinical models of triple-negative breast cancer (TNBC). SSTR2 expression in mouse samples was assessed via Western blot and immunohistochemistry. Real-time quantitative PCR (qRT-PCR), flow cytometry, and cell binding assays were utilized to determine if HDAC inhibition can upregulate SSTR2 expression. [^{68}Ga]Ga-DOTATATE positron emission tomography (PET) imaging, which targets SSTR2, was used to non-invasively characterize SSTR2 expression and variability in the EO771 and 4T1 TNBC models before and after HDAC inhibition. These studies demonstrate that HDAC inhibition can upregulate SSTR2 at the transcriptional, translational, and functional levels in breast cancer. Importantly, SSTR2 expression can be characterized non-invasively via PET imaging and modulation with HDAC inhibitors can be monitored longitudinally. Our findings highlight SSTR2 as a promising therapeutic molecular target in TNBC.

Keywords PET, Breast cancer, SSTR2, SAHA, HDAC, Preclinical

Breast cancer (BC) is the most common female cancer globally, with 10–20% of those cases being triple-negative[1,2]. TNBC, an aggressive and highly heterogeneous subtype of BC, is characterized by the absence of molecular targets found in other subtypes of BC including estrogen receptor (ER), progesterone receptor (PR), and HER2[3,4]. Due to the lack of therapeutic targets, there are currently no approved targeted therapies for patients with TNBC[4–6]. Current standard-of-care treatments have improved survival but are only effective in a small percentage of patients[7–9]. Therefore, identifying novel, targetable biomarkers in breast cancer are of interest.

Somatostatin receptors are overexpressed in some cancer tissues and there are clinically approved theranostic agents available for NETs. SSTR2 is a good potential molecular target for imaging and therapy due to its low expression in normal tissues[10,11]. PET imaging can non-invasively inform on molecular signatures within tumors, creating biomarkers of response or characterizing targets for therapy. Importantly, we can obtain

[1]Department of Radiology, The University of Alabama at Birmingham, VH G082, 1670 University Blvd, Birmingham, AL 35233, USA. [2]Graduate Biomedical Sciences, The University of Alabama at Birmingham, Birmingham, AL, USA. [3]Department of Chemistry, The University of Alabama at Birmingham, Birmingham, AL, USA. [4]Department of Surgery, The University of Alabama at Birmingham, Birmingham, AL, USA. [5]Department of Biomedical Engineering, The University of Alabama at Birmingham, Birmingham, AL, USA. [6]O'Neal Comprehensive Cancer Center, The University of Alabama at Birmingham, Birmingham, AL, USA. ✉email: asorace@uabmc.edu

quantitative metrics about underlying tumor biology to characterize tumors including glucose metabolism, cell proliferation, and receptor expression[12–15]. Specifically, SSTR2 expression can be evaluated non-invasively through PET imaging with the compound DOTATATE, a somatostatin analogue, which has high affinity for SSTR2[16]. Importantly, overexpression of SSTR2 can be targeted using theranostic approaches, which combines imaging with the delivery of therapy; currently, the radiotherapeutic [^{177}Lu]Lu-DOTATATE or LUTATHERA® is FDA-approved for use in NETs[11,17–21].

Clinically, patients with NETs which have high expression of SSTR2 (> 50% SSTR2 + from biopsy) are good candidates to receive targeted imaging and therapy with the FDA-approved somatostatin analogue radiopharmaceutical, LUTATHERA®[11,22]. Clinical trials are ongoing in hepatocellular carcinoma (NCT03648073), neuroblastoma (NCT05109728 and NCT03966651), meningioma (NCT03971461 and NCT04082520), and glioblastoma (NCT05109728), metastatic thyroid cancer (NCT04927416), and advanced or recurrent breast cancer (NCT04529044), highlighting the potential benefit of this target in other cancers. Some studies have found that SSTR2 expression strongly correlates with estrogen and progesterone hormone receptors, but expression is highly variable due to inter- and intra-tumoral heterogeneity[23–26]. To date, there have been a limited number of studies which suggest some subtypes, primarily luminal (ER + and or PR +) breast cancers, overexpress SSTR2, but there are a relatively limited number of case studies looking at SSTR2 expression[27–30]. Our study aims to characterize SSTR2 expression as a biomarker for targeted imaging and therapy in preclinical models of triple-negative breast cancer.

As promising as SSTR2 is as a target, many patients with breast cancer do not overexpress SSTR2 and expression is variable across studies[31,32]. However, histone deacetylase (HDAC) inhibitors have been shown to upregulate SSTR2 expression and therapeutic modulation can provide a potential target for imaging and therapy[33]. HDAC inhibitors prevent the removal of acetyl groups from histones, thereby leaving these histones transcriptionally active and epigenetically altering downstream pathways[34,35]. Notably, the use of HDAC inhibitors to upregulate SSTR2 expression has been well-established at the transcriptional, translational, and functional levels in neuroendocrine models[10,33,36–39]. Not only can HDAC inhibitors upregulate SSTR2 for imaging, but these drugs are also known to sensitize aggressive, invasive tumors to radiation therapy by repressing DNA repair pathways, thereby inducing cancer cell death[7,35,40,41]. There are currently many clinical trials exploring the combination of HDAC inhibitors with radiation therapy[42–49]. Taken together, these studies and our data presented in this manuscript highlight the potential synergy and benefits HDAC inhibition may have in combination with radiotherapy in triple-negative breast cancer.

Our study aimed to characterize SSTR2 expression in preclinical models of TNBC, in addition to investigating the potential of HDAC inhibitors to upregulate SSTR2 to serve as a biomarker for targeted imaging and therapy in tumors with low or variable basal expression. We initially quantified baseline levels of SSTR2 in two syngeneic models of breast cancer and demonstrated how HDAC inhibition can upregulate SSTR2 expression at the mRNA, protein, and protein-binding levels, thereby creating a molecular target for imaging and targeted radiotherapy. Additionally, we have investigated the feasibility of quantifying SSTR2 expression in breast cancer models non-invasively via PET imaging before and after HDAC inhibitor treatment. HDAC inhibitors have potential to upregulate SSTR2 expression as a biomarker of interest for image-guided delivery of radiotherapy to improve treatment response and reduce off-target therapeutic effects. Our approaches have the potential to be highly translational, with application in clinically relevant models. These studies have future clinical impact to provide a novel, targetable molecular approach to increase therapeutic response and improve survival for patients with difficult to treat breast cancer tumors.

Materials and methods

Cell culture

4T1, EO771, and TS/A mouse mammary carcinoma cells and H727 pulmonary NET cells were purchased from American Type Culture Collection (ATCC Manassas, VA). Cells were cultured in either RPMI 1640 medium (4T1) or phenol-free DMEM (EO771, TS/A) (Thermo Fisher Scientific, Waltham, MA) supplemented with 10% (v/v) fetal bovine serum (FBS, Biotechne S12450H), 1% (v/v) penicillin/streptomycin, 1% (v/v) sodium pyruvate, and 1% (v/v) L-glutamine and grown at 37 °C with 5% CO_2. Cells were cultured to 70–80% confluency and all cell counts were determined using a hemocytometer (Hausser Scientific) with trypan blue dye (Thermo Fisher Scientific Inc., Waltham, MA) exclusion to assess cell viability. 4T1 and EO771 TNBC cell lines were confirmed for ER-/PR-/HER2-expression via Western blot.

qRT-PCR to quantify mRNA expression of SSTR2

RNA samples were isolated from EO771 and 4T1 cells using RNeasy Plus Mini kit (Qiagen, Hilden, Germany). RNA concentrations were determined using a NanoDrop 1000 spectrophotometer (Thermo Fisher Scientific). RNA samples which have the ratio of absorbance at 260 nm and 280 nm greater than 2.0, deemed as sufficient RNA purity, were used in the experiments. Complementary DNA (cDNA) was synthesized using iScript RT Supermix (Bio-Rad 1708841) and 1 µg total RNA was used in each sample. PCR samples were prepared using SYBR Green master mixes (Bio-Rad 1725150). Real-time quantitative PCR was performed in triplicate on CFX Connect Real-Time PCR Detection System (Bio-Rad). The sequences of the PCR primers used for the analysis of mRNA expression of SSTR2 in this experiment are forward: CAAGCAATGGCTCCAACCAGAC, reverse: C TTGGCATAGCGGAGGATGACA (Origene MP215984). Target gene expression was normalized to GAPDH, and the ΔΔCt method[50] was used to calculate relative fold changes in gene expression.

Flow cytometry to quantify cell surface SSTR2 expression

Cultured EO771 and 4T1 cells (2.5×10^5) were seeded in 12-well plates, allowed to adhere overnight, then treated with varying doses (0–15 µM) of suberoylanilide hydroxamic acid (SAHA, Sigma Aldrich SML0061) or 0.2%

(v/v) dimethyl sulfoxide (DMSO, Fisher Scientific BP231-100) as a control diluted in growth medium for 24 h. After 24 h, media was aspirated, and cells were washed with 1X phosphate-buffered saline (PBS, Gibco 10–010-049) and isolated using 0.25% (v/v) Trypsin (Corning 25–054-CI). Trypsin was neutralized using complete growth medium and cell viability was assessed via trypan blue exclusion method. For each sample, 5×10^5 cells were then resuspended in fluorescent-associated cell sorting (FACS) buffer consisting of 1% (v/v) bovine serum albumin (BSA, Sigma Aldrich A4737), 1% (w/v) sodium azide (Sigma Aldrich S2002) in 1X PBS (Gibco 10–010-049). Cell surface staining was performed using fluorophore-conjugated antibodies incubated at 4 °C for 30 min in the dark. Antibodies include the following: LIVE/DEAD-NIR (Thermo Fisher L34975, 1:150 dilution) and FITC-SSTR2 (Novus 402038, 1:32 dilution). Following cell staining, two wash procedures were performed using 1X FACS buffer before final resuspension and data acquisition. Data was acquired using an Attune NxT flow cytometer (Thermo Fisher Scientific) and subsequent analysis was performed with FlowJo version 10.6.2 software.

Western blot to quantify SSTR2 protein levels

Cell lysates from mouse mammary carcinoma (TNBC EO771, TNBC 4T1, ER + TS/A) cells and H727 NET cells as a positive control were isolated using radio-immunoprecipitation (RIPA) lysis buffer with added protease inhibitors and phosphatase inhibitors (Pierce 89900, A32953, A32957). Protein concentrations were determined using Pierce Gold BCA Protein Assay Kit (Thermo Fisher Scientific A53226). Samples were prepared with 4X lithium dodecyl sulfate (LDS) sample buffer (Fisher Scientific NP0007) and contained 20 µg of total protein. Prior to gel electrophoresis, samples were heated at 95 °C for 10 min and centrifugated for 30 s. Samples and molecular weight markers were loaded into Mini-PROTEAN TGX precast gels (BioRad 4561096) and run at 100 V for 90 min. Proteins were transferred to Midi 0.2 µm polyvinyl difluoride (PVDF) membranes (BioRad) using the Trans-Blot Turbo Transfer System (BioRad) Standard Molecular Weight protocol for 30 min. Antibodies were diluted in 5% non-fat milk and dilutions include the following: SSTR2 mouse monoclonal antibody (A-8) with a dilution of 1:500 (Santa Cruz sc-365502), horseradish peroxidase (HRP)-conjugated monoclonal anti-mouse antibody with a dilution of 1:1000 (Cell Signaling Technology 7076s), and HRP-conjugated mouse monoclonal anti-beta actin antibody [AC-15] with a dilution of 1:2000 (Abcam ab49900). Molecular weight markers include MagicMark™ XP Western Protein Standard (Thermo Fisher LC5602) and Precision Plus Protein™ WesternC™ (BioRad 1610376). Western blot semi-quantitative values were obtained using ImageJ and SSTR2 expression (67–87 kDa) was normalized to the loading control beta-actin (42 kDa) and referred to in terms of relative intensity as previously reported[51].

[^{68}Ga]Ga-DOTATATE/[^{52}Mn]Mn-DOTATATE synthesis and radiolabeling

For all studies DOTA–d-Phe–Cys–Tyr–d–Trp–Lys–Thr–Cys-Thr (Macrocyclics C-220), or DOTATATE, was purchased commercially and was dissolved in water at a concentration of 5 mg/mL. To produce [^{68}Ga]Ga-DOTATATE, a ^{68}Ge/^{68}Ga generator (Eckert & Ziegler, Berlin, Germany) was eluted with 10 mL of 0.1 M HCl at a rate of 1 mL per minute and concentrated on a Strata-X-C SCX cartridge (Phenomenex, Torrance, CA). After drying, the gallium-68 was eluted from the cartridge using 400 µL of acetone into a vial containing 300 µL NaOAc (0.5 M, pH 3.5), and 6.4 µL of DOTATATE. The labeling reaction vial was heated at 98 °C while shaking at 300 rpm for 10 min. Radiochemical purity was assessed using instant thin layer chromatography (iTLC) paper and run in 50% (v/v) methanol and 5% (w/v) ammonium acetate in water on an AR-2000 Imaging Scanner (Eckert and Ziegler, MA, USA).

To create [^{52}Mn]Mn-DOTATATE, manganese-52 was produced through ^{nat}Cr(p,n)^{52}Mn nuclear reaction by irradiation of natural chromium targets on a TR24 cyclotron, as previously reported[52,53]. Following purification through ion exchange chromatography, 3.7 MBq (100 µCi) of [^{52}Mn]$MnCl_2$ was added to a vial containing 100 µL ammonium acetate (0.25 M, pH 4.5) and 5.5 nmol of DOTATATE. The labeling reaction vial was heated at 90 °C while shaking for 30 min. Radiochemical purity was assessed using instant thin layer chromatography (iTLC) analysis by using sodium citrate (0.1 M, pH 5) as mobile phase, as previously reported[54].

Cell binding assays to evaluate uptake of clinically relevant somatostatin analogues

Cells (2.5×10^5) were seeded in 12-well plates, allowed to adhere overnight, then treated with varying doses (0–15 µM) of suberoylanilide hydroxamic acid (SAHA, Sigma Aldrich SML0061) diluted in growth medium. After 24 h, media was aspirated, and cells were washed with 1X phosphate-buffered saline (PBS, Gibco 10–010-049). PBS was replaced with a solution containing 10 nM DOTATATE in growth medium and incubated at 37 °C for 1 h. After 1 h, cells were washed twice with 1X PBS and lysed using 200 µL NaOH. Cell lysates were transferred to 1.5 mL Eppendorf tubes for analysis on a Hidex Gamma Counter (Turku, Finland) and read for 1 min each to determine [^{52}Mn]Mn-DOTATATE uptake. Subsequently, protein concentrations for each lysate were determined using Pierce Gold BCA Protein Assay Kit to normalize DOTATATE uptake per milligram of protein.

Animal models and treatment schema

All animal work was performed in accordance with guidelines and regulations of UAB's Institutional Animal Care and Use Committee (IACUC) and Animal Resources Program (ARP). This facility is state-licensed and fully accredited by the American Association for Accreditation of Laboratory Animal Care (AAALAC). All procedures using animal subjects are approved by UAB's IACUC under animal protocol number (APN) 08778. Reporting of experiments using animal subjects are compliant with ARRIVE guidelines.

All procedures using animal subjects including housing, tumor inoculation, treatment administration, imaging, anesthesia via isoflurane, euthanasia via primary over-administration of 5% isoflurane and secondary cervical dislocation, and collection of biological materials are approved under APN 08778. Animals were

anesthetized during tumor inoculation, radiopharmaceutical administration, and imaging procedures. 5×10^5 EO771 cells in 20% Matrigel (Corning 356234) and saline or 2×10^5 4T1 cells in saline were implanted into the third mammary fat pad of female C57BL/6 or BALB/c mice, respectively. Mice bearing EO771 or 4T1 TNBC tumors entered the study upon reaching tumor volumes of 100–300 mm^3, referred to as day 0. Mice were randomized into treatment groups using a random number generator with quality checks to ensure equal tumor volume distributions between groups at baseline. Mice were treated with either saline control (n = 4) or single-agent SAHA (n = 12 EO771, n = 17 4T1) every 3 days via intraperitoneal injection beginning on Day 0. Dosing strategies of HDACi include 25 mg/kg suberoylanilide hydroxamic acid (SAHA, Sigma Aldrich SML0061) for EO771 tumor-bearing mice and 50 mg/kg 4T1-tumor bearing mice based on IC_{50} concentrations. Endpoints for tumor-bearing animals include sustained tumor volume of 2000 mm^3, 20% loss of body weight, or euthanasia at pre-determined time points of interest for biological validation.

[^{68}Ga]Ga-DOTATATE-PET/CT imaging and analysis

Mice were imaged with [^{68}Ga]Ga-DOTATATE, a radiolabeled somatostatin analogue which binds with the highest affinity to SSTR2, on day 0 and 7 of treatment, respectively. Tumor-bearing mice (n = 16 for EO771, n = 21 for 4T1) received 100 ± 20 µCi [^{68}Ga]Ga-DOTATATE (1 µg) formulated with sterile saline to a final injection volume of 100 µL per mouse. To allow time for accumulation in tissues of interest, doses circulated systemically for 60 min and then a 20-min Ga-68 static PET image was obtained followed by a 5-min computed tomography (CT 80 kVp) scan. PET/CT images were acquired using a GNEXT preclinical µPET/CT (SOFIE, Culver City, CA). PET images were reconstructed using a 3D OSEM algorithm with attenuation corrections and CT images were reconstructed using modified Felkamp algorithm. Regions of interest (ROIs) were drawn based on the anatomical CT reference images. Imaging occurred at baseline and 24 h following treatment with the pan-HDAC inhibitor SAHA. Mean and frequency histograms of standardized uptake value (SUV) were quantified using VivoQuant, a preclinical image processing software (v.4.0; Boston, MA). SUVs were calculated using the following formula: $SUV = C / (dose/weight)$ where C is the tissue radioactivity concentration, *dose* is the injected dose, and *weight* is body weight of the mouse in grams. Background ROIs were drawn in the left atrium and contralateral quadricep muscle of each animal for standard tissue to normalize SUV uptake in the tumor. Kidney and blood SUV uptake and quantification was performed to evaluate secondary kinetics. Histogram data of voxel-wise SUV metrics from the tumor was converted to frequency data (normalized by number of voxels per tumor) and analyzed to quantify average uptake in high expression regions, as previously reported[55].

Immunohistochemical analysis to quantify tumor SSTR2 expression

Tumor samples were collected and fixed with 10% buffered formalin overnight at room temperature. Paraffin embedding and 5 µm-thick slicing of tumor samples were performed in the UAB Pathology Core Research Lab. Hematoxylin and eosin (H&E) staining was performed as previously reported[56]. Immunohistochemical (IHC) analysis was performed to assess SSTR2 expression. Paraffin was removed using xylene (Fisher HC-700-1GAL) and slides were rehydrated through gradual ethanol dilution. Antigen retrieval was performed by microwaving slides at 100 °C for 10 min in 1X citrate buffer (Abcam ab93678). Slides were incubated in 3% H2O2 to block endogenous peroxidase activity and non-specific binding was prevented using blocking buffer composed of 1X PBS with 3% serum (w/v) and 0.3% (w/v) Triton X-100 (Sigma Aldrich X100-5ML). Primary antibody for anti-somatostatin receptor 2 (Anti-somatostatin receptor 2 [UMB1] C-terminal, Abcam ab134152) was diluted 1:200 in blocking buffer and incubated overnight at 4 °C. The next day, slides were incubated for 1 h at room temperature with secondary antibody diluted 1:500 in blocking buffer (Goat anti-rabbit IgG, Pierce 31820). Subsequently, slides were incubated in HRP-conjugated streptavidin (ThermoFisher N100) diluted 1:10,000 for 30 min at room temperature and developed using DAB (3,3'Diaminobenzidine) substrate exposure for 2 min (Abcam ab64238). Negative controls for the immunostaining procedure were conducted by omission of the primary antibody. Slides were imaged using EVOS M7000 system and subsequent analysis of positive IHC staining of the whole section was completed through automated MATLAB algorithms, as previously reported[57]. IHC samples were auto-segmented and images were transformed from RGB to HSV color space followed by the application of a saturation mask. Otsu's method was applied to separate positive from negative staining and the percentage of positive staining was defined as: *% positive staining = (total no. positively stained pixels) ÷ (total no. tumor pixels with noise and background removed) X 100.*

Statistical analysis

An independent t-test was used to determine differences between EO771 and 4T1 models. A one-way independent ANOVA with Bonferroni correction was used to assess differences in treatment groups for transcriptional, translational, and functional analyses. Differences across treatment groups and differences in imaging metrics were assessed using a non-parametric independent t-test. Differences between days including imaging metrics, body weight, and Log-rank tests were performed to determine differences in overall survival curves compared to control for each model. P values < 0.05 were considered significant.

Results

Baseline expression of SSTR2 varies across mouse mammary carcinoma cell lines

Basal SSTR2 expression varied among mouse mammary carcinoma cell lines but did show positive expression at some level in each breast cancer cell line (Fig. 1a). SSTR2 (~ 76 kilodaltons, kDa) was expressed at relatively low levels in 4T1 (0.43 RU, relative unit) and TS/A (0.36 RU) cells when normalized to beta-actin (42 kDa). SSTR2 expression for EO771 cells was 1.01 relative units and which was comparable to the positive control, H727 at 1.36. (Fig. 1a). Full length Western blot data for SSTR2 shows a range of sizes for SSTR2, which we attribute to post-translational modifications, including glycosylation, and the formation of homo- and hetero-dimers among

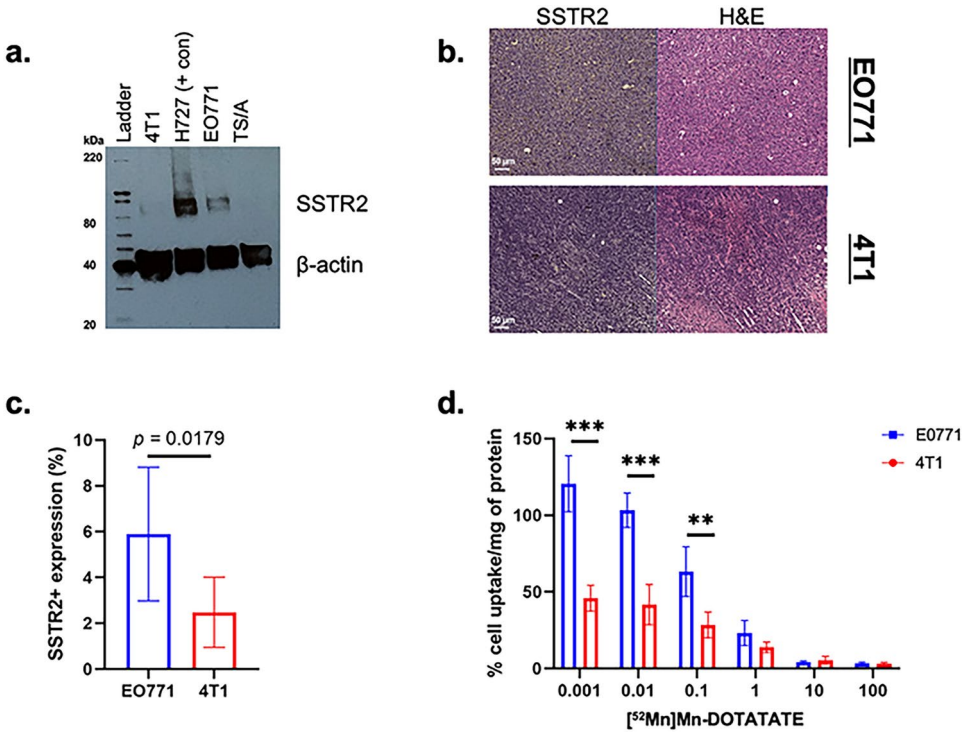

Fig. 1. Baseline SSTR2 expression varies in mouse mammary carcinoma cell lines. (**a**) Representative Western blot showing mouse mammary carcinoma cell lines basal expression of SSTR2 (~ 76 kDa) relative to β-actin (42 kDa). ThermoFisher MagicMark XP ladder is in the left lane and H727 pulmonary NET cells are used as a positive control. (**b**) Immunohistochemical data showing somatostatin expression in untreated syngeneic EO771 (top) and 4T1 (bottom) mouse breast cancer tumors with matched hematoxylin and eosin slides. Scale bar represents 50 µm. (**c**) Quantification of SSTR2 IHC staining in untreated EO771 and 4T1 tumors via MATLAB code (n = 7). (**d**) Cellular uptake of [^{52}Mn]Mn-DOTATATE shows EO771 cells have significantly higher uptake compared to 4T1 cells ($p = 0.0003$ for 0.001, $p = 0.0004$ for 0.01, $p = 0.0087$ for 0.1). Uptake was normalized to milligram of protein and represented as % cell uptake/mg of protein (n = 4 per group).

subtypes, in addition to plasma membrane and cytosolic fractions of this receptor, which have been reported previously[58,59]. Current literature in NETs demonstrates that HDAC inhibitors can modulate SSTR2 expression even in cell lines with moderate basal expression, such as H727[36,37]. We observed that EO771 cells had similar basal expression to H727 cells, and even less in 4T1 cells. Therefore, 4T1 and EO771 TNBC cells were chosen as the primary lines of interest to further characterize modulation of SSTR2 expression. To determine whether SSTR2 is expressed in vivo we performed immunohistochemistry staining of SSTR2 in untreated EO771 and 4T1 tumors (Fig. 1b). We observed similarly to in vitro data, that EO771 tumors had relatively high SSTR2 expression and 4T1 tumors had low expression. Quantification of SSTR2 staining via custom-made MATLAB code showed that EO771 tumors had significantly increased SSTR2 compared to 4T1 tumors, as previously described[57]. Quantification also showed that SSTR2 expression was heterogeneous for both models (Fig. 1c). Finally, we determined cell uptake of DOTATATE, a clinically relevant somatostatin analogue which binds with high affinity to human SSTR2. We performed a cell binding assay with EO771 and 4T1 cells at different concentrations of DOTATATE radiolabeled with Mn-52 (Fig. 1d). Cellular uptake of [^{52}Mn]Mn-DOTATATE shows that EO771 cells have significantly higher uptake compared to 4T1 cells at 0.001 µg ($p = 0.0003$), 0.01 µg ($p = 0.0004$), and 0.1 µg ($p = 0.0087$) of DOTATATE. In addition, the binding assay demonstrated the potential for targeted imaging of SSTR2 as a biomarker for breast cancer in vivo. Taken together, these results suggest that EO771 tumors have higher expression of SSTR2 compared to 4T1 tumors. Overall, SSTR2 is expressed in syngeneic murine breast cancer cell lines and though expression is heterogeneous, SSTR2 may be a promising biomarker for imaging and therapy in breast cancer.

PET imaging reveals differences in SSTR2 expression among murine breast cancer models

After establishing basal expression of SSTR2 in murine TNBC cell lines and tissues, [^{68}Ga]Ga-DOTATATE PET imaging was utilized to determine whether SSTR2 in breast cancer can be evaluated non-invasively in vivo. [^{68}Ga]Ga-DOTATATE imaging demonstrated that both EO771 and 4T1 tumors have tracer uptake in naïve, untreated animals, and that EO771 tumors had visually higher uptake compared to 4T1 tumors (Fig. 2a). Frequency histograms of the distribution of [^{68}Ga]Ga-DOTATATE were used to compare model-dependent differences in SSTR2 expression across the entire tumor while accounting for potential differences in tumor volume. Histogram analysis revealed high heterogeneity of SSTR2 in EO771 and 4T1 tumors, as seen by wide shifts in the frequency histograms for each model (Fig. 2b). The distribution of DOTATATE uptake for

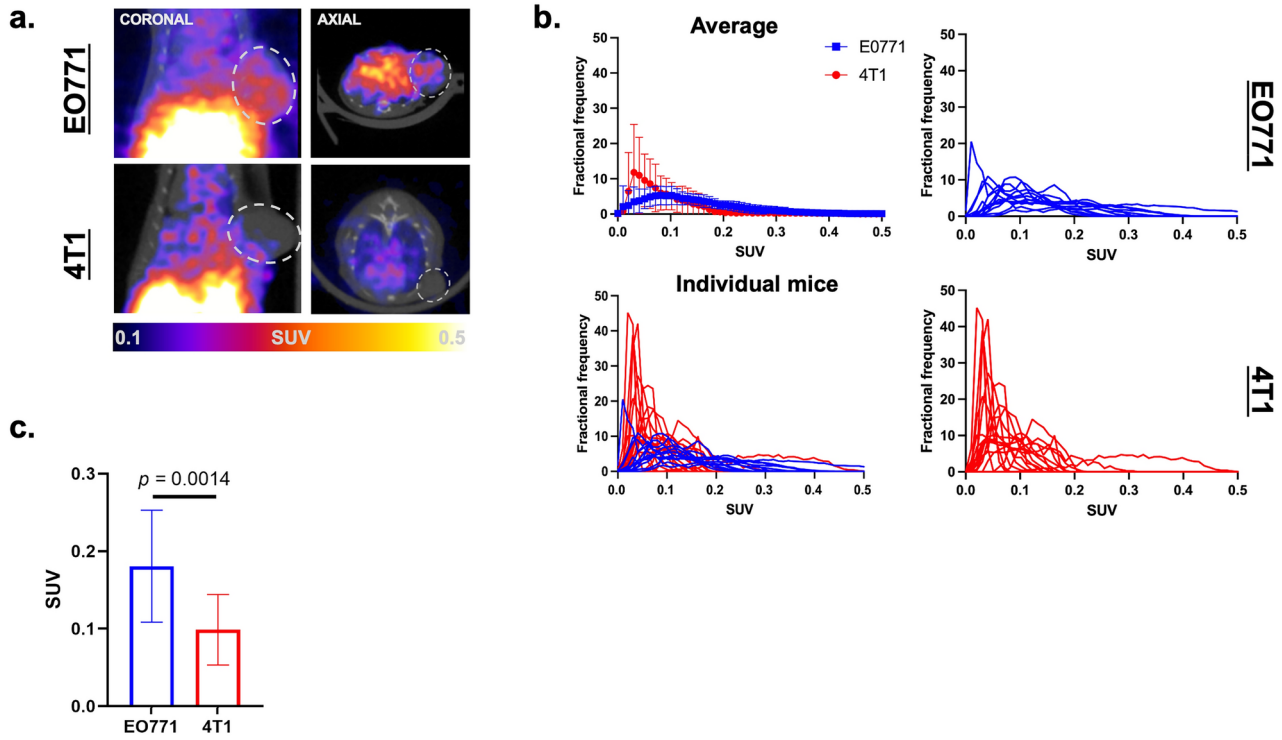

Fig. 2. PET imaging reveals model-dependent differences in SSTR2 expression. (**a**) Representative images from EO771 and 4T1 tumor-bearing mice taken 60-min post-injection of 100 ± 20 µCi [^{68}Ga]Ga-DOTATATE on day 0. ROIs encircling tumors are represented by grey dotted circles. (**b**) Frequency histogram distributions for [^{68}Ga]Ga-DOTATATE uptake in EO771 and 4T1 tumors are represented as the average ± standard deviation, comparison of the two models, and individual animals from each model. (**c**) SUV values are significantly higher for EO771 tumors compared to 4T1 tumors in the top 10% ($p = 0.0014$) of frequency distributions (n = 12 for EO771, n = 17 for 4T1).

both models was platykurtic, however, the distribution in 4T1 tumors was positively skewed compared to the distribution in EO771 tumors (Fig. 2b). Evaluating the highest voxels within the tumor frequency distributions demonstrated that EO771 tumors have significantly higher SUV in the top 10% (left, $p = 0.0014$) of their distributions compared to the 4T1 model (Fig. 2c). Overall, PET imaging showed that EO771 tumors had higher expression of SSTR2 at baseline compared to 4T1 tumors, but both tumor models show heterogeneity in their distributions for SSTR2 expression.

Expression of SSTR2 can be upregulated by treatment with HDAC inhibition at the transcriptional, translational, and functional levels

We determined the cytotoxic effects of HDAC inhibition on murine triple-negative breast cancer cell lines and established the half-maximal inhibitory concentration (IC_{50}) of the pan-HDAC inhibitor, suberoylanalide hydroxamic acid (SAHA), to be 3.53 µM for EO771 cells and 17 µM for 4T1 cells (Supplemental Fig. 1). Following establishment of IC50 concentrations, we performed in vitro assays to determine the effects of SAHA on SSTR2 expression in both syngeneic models at the transcriptional, translational, and functional levels. qRT-PCR revealed that SAHA treatment increases transcriptional expression of SSTR2 compared to control by up to 4 × for EO771 (Fig. 3a, $p < 0.0001$ for 1.7 µM and 3.3 µM) and up to 8 × for 4T1 (Fig. 3b, $p = 0.001$ for 3 µM, $p = 0.0009$ for 5 µM). SSTR2 is upregulated transcriptionally by treatment with HDAC inhibitors, particularly SAHA. Western blot analysis revealed that whole cell protein expression of SSTR2 increases with increasing doses of SAHA for both EO771 and 4T1 cell lines (Supplemental Fig. 2). Mean fluorescent intensity of SSTR2 from flow cytometry assays shows significant increases in SSTR2 cell surface receptor expression after SAHA treatment for both EO771 (Fig. 3c, $p < 0.0001$) and 4T1 cells (Fig. 3d, $p = 0.0001$). SSTR2 protein expression was significantly increased by treatment with HDAC inhibitor, SAHA. Using a cell binding assay with [^{52}Mn]Mn-DOTATATE, EO771 cells showed significant increases in DOTATATE uptake up to 200% cell uptake per milligram of protein after treatment with SAHA for 24 h (Fig. 3e, $p = 0.002$ for 1.7 µM, $p < 0.0001$ for 3.3 µM). 4T1 cells showed significant increases in uptake of DOTATATE after SAHA treatment with up to 120% cell uptake per milligram of protein (Fig. 3f, $p < 0.0001$ for 3 µM and 5 µM). Interestingly, the uptake of DOTATATE seemed to plateau for this cell line, suggesting there may be a maximal binding rate or receptor saturation. Cells pretreated with SAHA for 24 h showed significantly higher uptake of [^{52}Mn]Mn-DOTATATE, demonstrating increased expression of SSTR2 on the cell surface. Overall, our data confirmed that HDAC inhibition upregulates SSTR2 at the mRNA, protein, and protein-binding levels in two syngeneic cell lines.

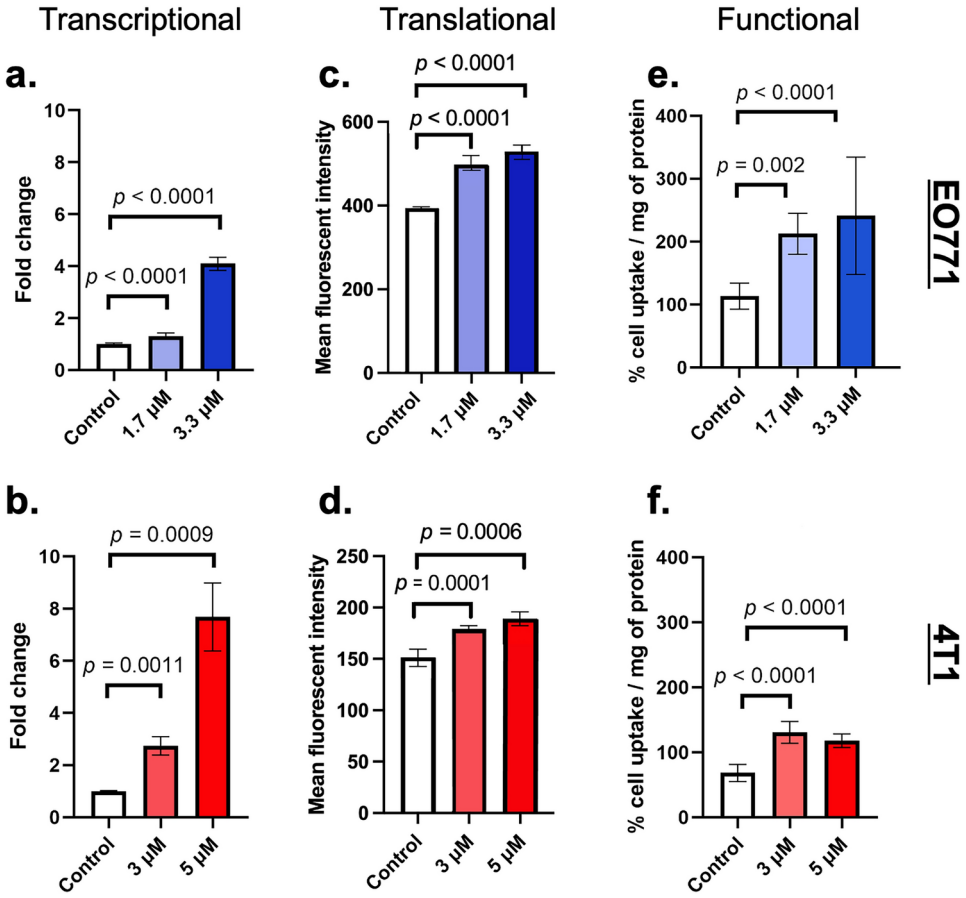

Fig. 3. SAHA increases expression of SSTR2 at the transcriptional, translational, and functional levels of two TNBC cell lines. (**a**) qRT-PCR shows 4 × increase ($p < 0.0001$ for 1.7 μM and 3.3 μM) in mRNA expression of *Sstr2* expression in EO771 cells treated with SAHA compared to control. (**b**) qRT-PCR shows 2 × change ($p = 0.001$ for 3 μM) and almost 8 × increase ($p = 0.0009$ for 5 μM) in *Sstr2* mRNA in 4T1 cells treated with SAHA compared to control. Flow cytometry demonstrates increased cell surface expression of SSTR2 for EO771 ($p < 0.0001$ for 1.7 μM and 3.3 μM) and 4T1 ($p = 0.0001$ for 3 μM, $p = 0.0006$ for 5 μM) cells following SAHA treatment compared to DMSO control (**c**, **d**). Cell binding assay with [^{52}n]Mn-DOTATATE shows increased uptake of somatostatin analogue in 4T1 ($p < 0.0001$ for 3 μM and 5 μM) and EO771 ($p = 0.002$ for 1.7 μM, $p < 0.0001$ for 3.3 μM) cells compared to DMSO control after HDACi for 48 h (**e, f**).

HDAC inhibitor treatment increases SSTR2 expression and overall survival in vivo

Representative PET images of EO771 and 4T1 tumors before and after treatment with SAHA can be seen in Fig. 4a showing increased uptake of somatostatin analogue, [^{68}Ga]Ga-DOTATATE, for both models. Quantification of [^{68}Ga]Ga-DOTATATE metrics shows increases in SUV_{mean}, SUV_{max}, and tumor-to-background ratios (TBR) for both EO771 and 4T1 tumors following SAHA treatment (Supplemental Table 1). SUV_{max} uptake normalized to muscle (SUV_{max}:muscle) was increased yet did not reach significance in EO771 tumors ($p = 0.0583$) following treatment with SAHA (Fig. 4b). 4T1 tumors treated with SAHA had significantly increased SUV_{max}:muscle ($p = 0.014$) ratios compared to baseline (Fig. 4e). To assess HDAC inhibitor-induced changes following SAHA treatment and account for tumor volume and heterogeneity, we quantified frequency histograms and compared the top 10% of the distributions. [^{68}Ga]Ga-DOTATATE uptake was significantly higher after treatment with SAHA in EO771 tumors (Fig. 4c, $p = 0.0113$) and 4T1 tumors (Fig. 4f, $p = 0.045$). Following the imaging study, we determined if HDAC inhibitors effectively influence overall survival. EO771 and 4T1 tumor-bearing mice receiving saline as a control or HDAC inhibitor treatment were assessed for survival or until reaching a tumor volume of 2000 mm^3. Treatment with SAHA significantly increased overall survival for both EO771 (Fig. 4d, $p = 0.0043$) or 4T1 (Fig. 4g, $p = 0.023$) tumor-bearing mice compared to control groups.

Assessing toxicity of HDACi and DOTATATE in models of triple-negative breast cancer

Additional analyses was performed to assess potential nephrotoxicity of SAHA and DOTATATE, as a small number of studies have reported potential nephrotoxicity and increased kidney retention of radiotracer[60,61]. Through image analysis of the kidneys, we identified no increase in kidney retention of the radiopharmaceutical for SAHA-treated animals compared to control in the EO771 model (Fig. 5a, $p = 0.4478$) or 4T1 model (Fig. 5c, $p = 0.513$). To determine potential differences in circulation and clearance of [^{68}Ga]Ga-DOTATATE, we quantified

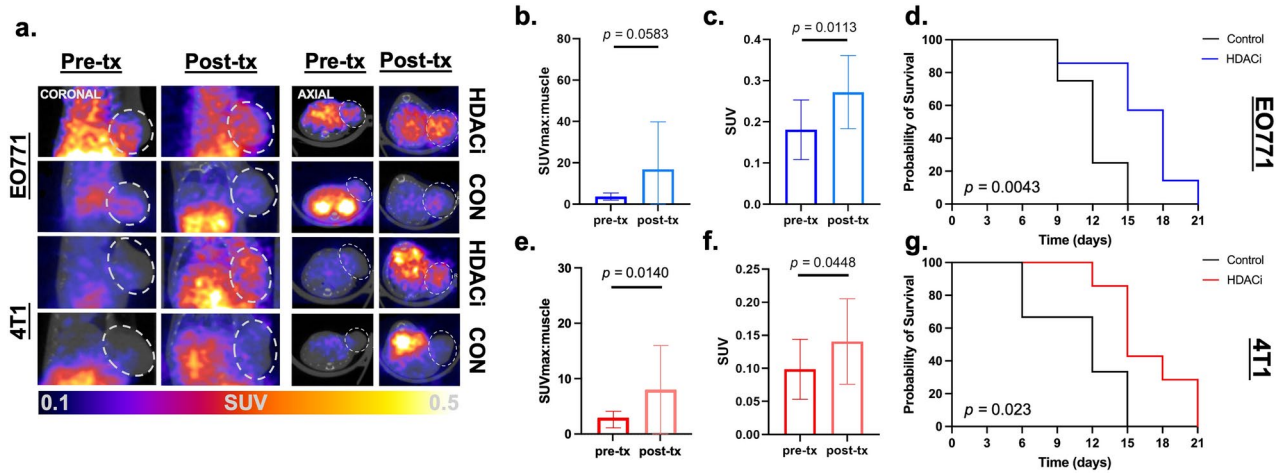

Fig. 4. HDAC inhibition increases SSTR2 expression and overall survival in vivo. (**a**) Representative images from EO771 and 4T1 tumor-bearing mice at day 0 and 7 of treatment with SAHA (n = 12 EO771, n = 17 4T1) or saline for control animals (n = 4) taken 60-min post-injection of 100 ± 20 µCi [^{68}Ga]Ga-DOTATATE. (**b**) Quantification of the highest voxel, SUV_{max}, of [^{68}Ga]Ga-DOTATATE uptake normalized to muscle is significantly increased in EO771 tumors following treatment with SAHA ($p = 0.0583$). (**c**) Quantification of SUV shows that radiotracer uptake is significantly higher after treatment with SAHA in the top 10% (right, $p = 0.0113$) of the frequency distribution for EO771 tumors. (**e**) [^{68}Ga]Ga-DOTATATE SUV_{max} normalized to heart and muscle is significantly increased in 4T1 tumors following treatment with SAHA ($p = 0.014$). (**f**) SUV uptake in the top 10% ($p = 0.0448$) of the distribution is significantly increased after SAHA treatment in 4T1 tumors. Overall survival is significantly increased for animals with EO771 tumors (**d**, $p = 0.0043$) and 4T1 tumors (**g**, $p = 0.023$) treated with SAHA.

tracer SUV_{mean} of uptake in the heart. We observed no difference in uptake in the heart for animals in the EO771 model (Fig. 5b, $p = 0.8961$) or 4T1 model (Fig. 5d, $p = 0.4869$). Body weight was continually monitored as an overall measure of animal health. We observed and no significant loss of body weight for EO771 tumor-bearing animals receiving saline as a control (Fig. 5e, $p = 0.38$) or SAHA (Fig. 5f, $p = 0.26$). Similarly, we observed no loss of body weight for 4T1 tumor-bearing animals treated with saline (Fig. 5g, $p = 0.10$), but observed weight gain in our animals treated with SAHA (Fig. 5h, $p = 0.006$). Though we did not specifically test for cardiotoxicity or nephrotoxicity, we utilized tracer retention in the heart and kidneys as a surrogate measure and observed no significant changes in [^{68}Ga]Ga-DOTATATE uptake. Future work to fully characterize the potential off-target effects is necessary to ensure the safety of these therapies. Overall, HDAC inhibition with SAHA in combination with DOTATATE imaging did not impact overall health of animals enrolled in the study, suggesting that this specific combination does not cause off-target effects or toxicities.

Discussion

Our studies revealed that SSTR2 is a potential molecular target for imaging and therapy in triple-negative breast cancer. SSTR2 expression can be induced and increased through HDAC inhibition, presenting a potential opportunity to deliver targeted therapy to tumors which lack typical molecular targets. Clinically, there is an established relationship between SSTR2 expression and hormone receptor status, leaving TNBC subsets with low and variable expression. Our findings show that the baseline expression of SSTR2 varies and is heterogeneous in mouse models of breast cancer. However, we have demonstrated that SSTR2 can be imaged in two breast cancer models and subsequently upregulated therapeutically with non-cytotoxic doses of the HDAC inhibitor, SAHA. These results suggest that epigenetic modulation of SSTR2 using HDAC inhibitors is a viable targeted strategy for imaging and therapy in breast cancers which have low or variable levels of SSTR2. Notably, treatment with SAHA increased SSTR2 for both EO771 and 4T1 tumors, regardless of their initial SSTR2 expression. PET imaging with [^{68}Ga]Ga-DOTATATE allowed us to non-invasively evaluate the extent and heterogeneity of SSTR2 expression within the tumor. Importantly, we believe that the repurposing of targeted radiotherapy directed at SSTR2, such as LUTATHERA®, may offer potential to enhance disease management and alleviate disease burden for patients with SSTR2-overexpressing or HDAC-induced tumors. Our approaches support the potential for the application of these relatively novel therapies in breast cancer patients. Investigating these novel radiotherapies may provide new opportunities to identify specific subsets of breast cancer patients who may potentially benefit from SSTR2-targeted therapies.

Data collected in these studies suggests breast cancer tumors have similar modulation of SSTR2 to NETs, where HDAC inhibition upregulated SSTR2 expression in pancreatic, pulmonary, and thyroid NETs[36–38,61–63]. We observed increases in SSTR2 at the transcriptional, translational, and functional levels even in cell types that had high basal levels of expression. We observed significant increases in cellular uptake of DOTATATE in vitro for both EO771 and 4T1 cells when treated with SAHA, which can be attributed to relatively low total protein concentration (0.2 mg per well). Notably, there appears to be a plateau in SSTR2 expression for 4T1 tumors,

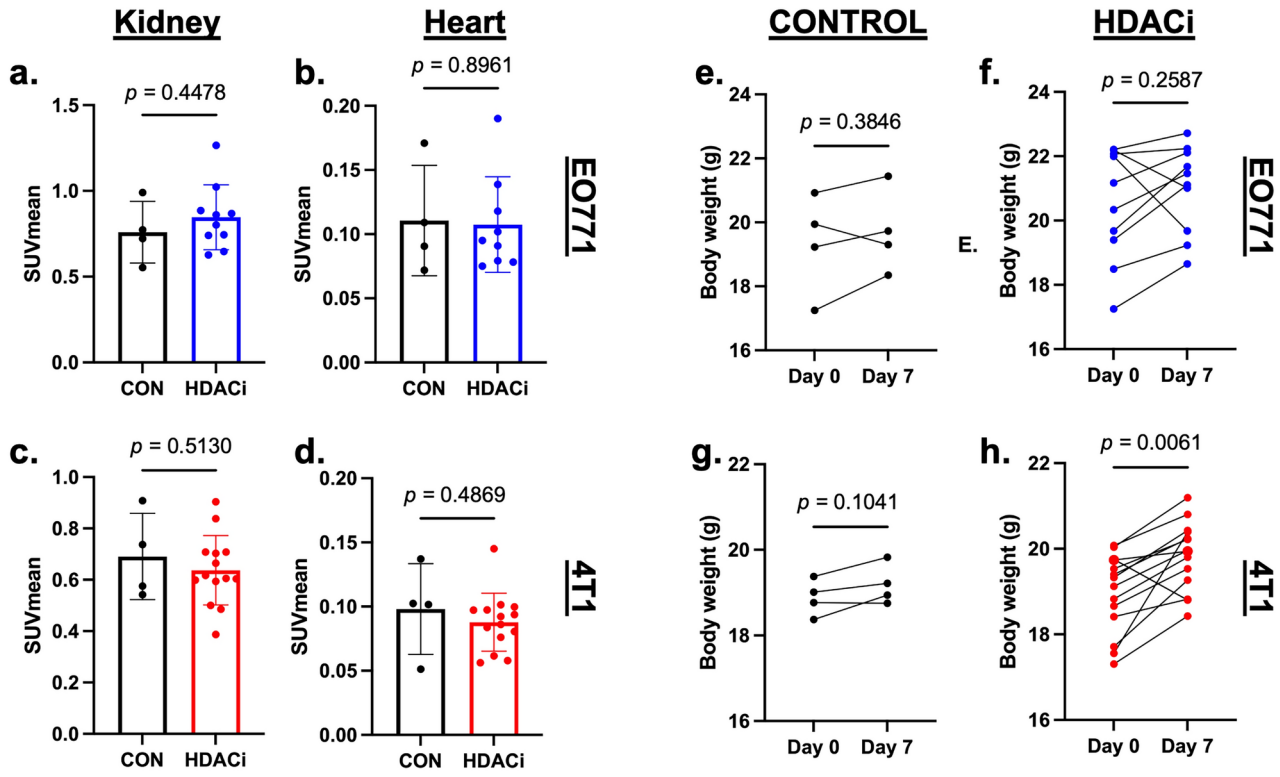

Fig. 5. Assessing toxicity of HDACi and DOTATATE in models of triple-negative breast cancer. (**a**) SUV_{mean} of [^{68}Ga]Ga-DOTATATE is not significantly different between control and SAHA-treated animals for EO771 tumor-bearing animals ($p = 0.4478$). (**b**) SUV_{mean} of tracer uptake in the heart is not significantly different between control and SAHA-treated animals in the EO771 model ($p = 0.8961$). (**c**) There is no significant difference in kidney SUV_{mean} between control and SAHA-treated animals in the 4T1 model. (**d**) SUV_{mean} of tracer uptake in the heart is not significantly different between control and SAHA-treated animals in the 4T1 model ($p = 0.4869$). Body weight of EO771 tumor-bearing mice is not significantly different for animals receiving **e.** saline as a control ($p = 0.3846$) or (**f**) SAHA treatment ($p = 0.2587$). Body weight of 4T1 tumor-bearing mice is not significantly different for animals receiving (**g**) saline as a control ($p = 0.1041$), but is increased for animals receiving (**h**) SAHA treatment ($p = 0.006$).

suggesting potential saturation of expression or receptor status which differs from NETs. Similarly to NETs, TNBC tumors had enhanced SSTR2 with increasing doses of HDAC inhibitors, suggesting SSTR2 expression is dose-dependent[37,64,65]. Therefore, designing treatment regimens and timing of HDAC inhibitor administration in reference to imaging or future theranostic studies is important.

Expression of SSTR2 was shown to vary greatly between tumor models and across various mouse cell lines. In addition, we have identified SSTR2 expression to be highly heterogeneous in syngeneic, preclinical breast cancer tumors. Similar observations about SSTR2 heterogeneity have been made in NETs and clinically in breast cancer[16,39,41]. The average distribution, or SUV_{mean}, showed decreases in standard deviations for both EO771 and 4T1 tumors following treatment with SAHA, suggesting potential increases in homogeneity which may improve the delivery of targeted radiotherapy. Heterogeneity of receptor expression is an important consideration in image-guided therapy and non-invasive evaluation via imaging plays a key role in determining eligibility for theranostic approaches. Importantly, SSTR2 expression was seen in a TNBC model (the 4T1) which is known to have a "cold" immune profile[66–68], suggesting the potential for use in tumors that do not respond well to immunotherapy. Literature has suggested that SSTR2 is expressed on some immune cell populations and that somatostatin receptors can stimulate immune responses[69–72]. Further studies are needed in these models to explore the roles that HDAC inhibition and SSTR2 expression may have in driving immune infiltration and response in triple-negative breast cancer.

One potential limitation in this study lies in the broad-acting nature of HDAC inhibitors and potential for off-target effects. However, suberoylanalide hydroxamic acid (SAHA), or Vorinostat, is a small molecule histone deacetylase inhibitor which has been FDA-approved for use in cutaneous T cell lymphoma. Vorinostat is being investigated for indications in other cancers including non-small cell lung carcinoma (NCT02638090), gliomas (NCT00268385, NCT00555399, NCT01236560), various lymphomas (NCT00392353, NCT031503290, melanoma (NCT01587352), and advanced breast cancer (NCT03742245, NCT00616967, NCT03878524)[73–75]. Additionally, many studies have demonstrated the strong anti-tumor activity of SAHA alone and in conjunction with other approved therapies in various cancer models including breast cancer[35,39,76,77]. Overall, there is great potential for HDAC inhibitors to provide strong anti-tumor responses and create molecular targets for imaging

and therapy. HDAC inhibitor treatment with valproic acid (VPA) and DOTATATE has been shown by Klomp et al. to have potential off-target effects and nephrotoxicity in preclinical models[60]. Another study has reported increased kidney retention, but did not further investigate potential toxicity of this high-dose HDAC inhibitor treatment[60,61]. VPA, clinically, has had rare side effects on renal function and has been implicated in neurological disorders[78]. However, this group and others have investigated alternative HDAC inhibitors, demonstrating the potential value of combining these therapies with radiotherapies to target SSTR2 overexpression[36,37,64,65]. While we did not observe any negative impact of HDAC inhibitor therapy, evidenced by the absence of significant weight changes, death, or retention of radiotracer in the kidney, we acknowledge the potential for signaling cascades to be affected downstream due to the epigenetic alterations induced by HDAC inhibitors.

Non-invasive PET imaging can inform on SSTR2 expression in preclinical models of breast cancer throughout the course of therapy. Further, imaging can be utilized to characterize and identify SSTR2 + tumors for targeted theranostic treatment. We aim to further explore the therapeutic upregulation of SSTR2 in vivo and repurpose clinically relevant theranostic agents for use in breast cancer. Our studies have characterized epigenetic induction of SSTR2 expression as a promising new molecular target for triple-negative breast cancer imaging and therapy. Translationally, therapeutic augmentation of SSTR2 serves as an opportunity to improve targeted imaging and therapy for patients with aggressive breast cancer who lack effective treatment options. Overall, employing HDAC inhibition to upregulate SSTR2 expression at the molecular level serves as a methodology which could reasonably provide a target for both imaging and therapy in breast cancer. Repurposing FDA-approved agents such as SAHA and LUTATHERA® could benefit patients who currently are not eligible for other targetable therapeutics. Translationally, the utilization of HDAC inhibitors and SSTR-targeted imaging and radiotherapy could provide a novel, targeted therapeutic approach for patients with triple-negative breast cancer.

Data availability

The datasets generated and analyzed during these studies are available from the corresponding author upon request.

Received: 19 April 2024; Accepted: 12 March 2025
Published online: 22 March 2025

References

1. Almansour, N. M. Triple-negative breast cancer: A brief review about epidemiology, risk factors, signaling pathways, treatment and role of artificial intelligence. *Front. Mol. Biosci.* **9**, 836417 (2022).
2. Howard, F. M. & Olopade, O. I. Epidemiology of triple-negative breast cancer: A review. *Cancer J.* **27**(1), 8–16 (2021).
3. Bianchini, G. et al. Triple-negative breast cancer: Challenges and opportunities of a heterogeneous disease. *Nat. Rev. Clin. Oncol.* **13**(11), 674–690 (2016).
4. Yin, L. et al. Triple-negative breast cancer molecular subtyping and treatment progress. *Breast Cancer Res.* **22**(1), 61 (2020).
5. Wahba, H. A. & El-Hadaad, H. A. Current approaches in treatment of triple-negative breast cancer. *Cancer Biol. Med.* **12**(2), 106–116 (2015).
6. Vagia, E., Mahalingam, D., & Cristofanilli, M. *The Landscape of Targeted Therapies in TNBC.* Cancers (Basel), 2020. **12**(4).
7. Furlanetto, J. & Loibl, S. Optimal systemic treatment for early triple-negative breast cancer. *Breast Care (Basel)* **15**(3), 217–226 (2020).
8. Korde, L. A. et al. Neoadjuvant chemotherapy, endocrine therapy, and targeted therapy for breast cancer: ASCO guideline. *J. Clin. Oncol.* **39**(13), 1485–1505 (2021).
9. Nofech-Mozes, S. et al. Patterns of recurrence in the basal and non-basal subtypes of triple-negative breast cancers. *Breast Cancer Res. Treat.* **118**(1), 131–137 (2009).
10. Hu, Y. et al. Role of somatostatin receptor in pancreatic neuroendocrine tumor development, diagnosis, and therapy. *Front. Endocrinol. (Lausanne)* **12**, 679000 (2021).
11. Hennrich, U., & Kopka, K. Lutathera((R)): The first FDA- and EMA-approved radiopharmaceutical for peptide receptor radionuclide therapy. *Pharmaceuticals (Basel)*, 2019. **12**(3).
12. Bashir, A. et al. In vivo imaging of cell proliferation in meningioma using 3'-deoxy-3'-[(18)F]fluorothymidine PET/MRI. *Eur. J. Nucl. Med. Mol. Imaging* **47**(6), 1496–1509 (2020).
13. Sorace, A. G. et al. Imaging for response assessment in cancer clinical trials. *Semin. Nucl. Med.* **50**(6), 488–504 (2020).
14. Ducharme, M., et al., *Evaluation of (68)Ga-radiolabeled peptides for HER2 PET imaging. Diagnostics (Basel)*, 2022. **12**(11).
15. Mason, C. et al. Novel tracers and radionuclides in PET imaging. *Radiol. Clin. North Am.* **59**(5), 887–918 (2021).
16. Fonti, R. et al. Heterogeneity of SSTR2 expression assessed by (68)Ga-DOTATOC PET/CT using coefficient of variation in patients with neuroendocrine tumors. *J. Nucl. Med.* **63**(10), 1509–1514 (2022).
17. Strosberg, J. et al. Phase 3 trial of (177)Lu-Dotatate for midgut neuroendocrine tumors. *N. Engl. J. Med.* **376**(2), 125–135 (2017).
18. Kurz, S.C., et al., *Evaluation of the SSTR2-targeted radiopharmaceutical 177Lu-DOTATATE and SSTR2-specific 68Ga-DOTATATE PET as imaging biomarker in patients with intracranial meningioma. Clin. Cancer Res.* (2023).
19. Herrera-Martinez, A. D. et al. Targeted systemic treatment of neuroendocrine tumors: Current options and future perspectives. *Drugs* **79**(1), 21–42 (2019).
20. Rivero, J. D. et al. Systemic therapy for tumor control in metastatic well-differentiated gastroenteropancreatic neuroendocrine Tumors: ASCO guideline. *J. Clin. Oncol.* **41**(32), 5049–5067 (2023).
21. Yamamoto, S. et al. The real-world selection of first-line systemic therapy regimen for metastatic gastroenteropancreatic neuroendocrine neoplasm in Japan. *Sci. Rep.* **12**(1), 17601 (2022).
22. Qian, Z. R. et al. Association between somatostatin receptor expression and clinical outcomes in neuroendocrine tumors. *Pancreas* **45**(10), 1386–1393 (2016).
23. Dalm, S. U. et al. Clinical relevance of targeting the gastrin-releasing peptide receptor, somatostatin receptor 2, or chemokine C-X-C motif receptor 4 in breast cancer for imaging and therapy. *J. Nucl. Med.* **56**(10), 1487–1493 (2015).
24. Frati, A. et al. Expression of somatostatin type-2 and -4 receptor and correlation with histological type in breast cancer. *Anticancer Res.* **34**(8), 3997–4003 (2014).
25. Reubi, J. C. et al. Somatostatin receptor incidence and distribution in breast cancer using receptor autoradiography: Relationship to EGF receptors. *Int. J Cancer* **46**(3), 416–420 (1990).
26. Kumar, U. et al. Somatostatin receptors in primary human breast cancer: quantitative analysis of mRNA for subtypes 1–5 and correlation with receptor protein expression and tumor pathology. *Breast Cancer Res. Treat.* **92**(2), 175–186 (2005).

27. Dude, I. et al. Evaluation of agonist and antagonist radioligands for somatostatin receptor imaging of breast cancer using positron emission tomography. *EJNMMI Radiopharm. Chem.* **2**(1), 4 (2017).
28. Fani, M. et al. Unexpected sensitivity of sst2 antagonists to N-terminal radiometal modifications. *J. Nucl. Med.* **53**(9), 1481–1489 (2012).
29. Dalm, S. U. et al. SSTR-mediated imaging in breast cancer: Is there a role for radiolabeled somatostatin receptor antagonists?. *J. Nucl. Med.* **58**(10), 1609–1614 (2017).
30. Evans, A. A. et al. Analysis of somatostatin receptor subtype mRNA expression in human breast cancer. *Br. J. Cancer* **75**(6), 798–803 (1997).
31. Priyadarshini, S., Allison, D.B., & Chauhan, A. Comprehensive assessment of somatostatin receptors in various neoplasms: A systematic review. *Pharmaceutics*, 2022. **14**(7).
32. Zou, Y. et al. Expression and selective activation of somatostatin receptor subtypes induces cell cycle arrest in cancer cells. *Oncol. Lett.* **17**(2), 1723–1731 (2019).
33. Klomp, M. J. et al. Epigenetic regulation of somatostatin and somatostatin receptors in neuroendocrine tumors and other types of cancer. *Rev. Endocr. Metab. Disord.* **22**(3), 495–510 (2021).
34. Wagner, J. M. et al. Histone deacetylase (HDAC) inhibitors in recent clinical trials for cancer therapy. *Clin. Epigenet.* **1**(3–4), 117–136 (2010).
35. Groselj, B. et al. Histone deacetylase inhibitors as radiosensitisers: effects on DNA damage signalling and repair. *Br. J Cancer* **108**(4), 748–754 (2013).
36. Guenter, R.E., et al., *Pulmonary carcinoid surface receptor modulation using histone deacetylase inhibitors. Cancers (Basel)*, 2019. **11**(6).
37. Klomp, M.J., et al., Comparing the effect of multiple histone deacetylase inhibitors on SSTR2 expression and [(111)In]In-DOTATATE uptake in NET cells. *Cancers (Basel)*, 2021. **13**(19).
38. Klomp, M. J. et al. Applying HDACis to increase SSTR2 expression and radiolabeled DOTA-TATE uptake: from cells to mice. *Life Sci.* **334**, 122173 (2023).
39. Shen, C. et al. HDAC inhibitors enhance the anti-tumor effect of immunotherapies in hepatocellular carcinoma. *Front. Immunol.* **14**, 1170207 (2023).
40. Meyskens, F.L., Jr., et al., Cancer prevention: Obstacles, challenges and the road ahead. J Natl Cancer Inst, 2016. **108**(2).
41. Karagiannis, D., & Rampias, T. HDAC inhibitors: Dissecting mechanisms of action to counter tumor heterogeneity. *Cancers (Basel),* 2021. **13**(14).
42. Shirbhate, E. et al. The combination of histone deacetylase inhibitors and radiotherapy: A promising novel approach for cancer treatment. *Fut. Oncol* **16**(30), 2457–2469 (2020).
43. Wang, H. et al. NK-/T-cell lymphomas. *Leukemia* **35**(9), 2460–2468 (2021).
44. Hontecillas-Prieto, L. et al. Synergistic enhancement of cancer therapy using HDAC inhibitors: Opportunity for clinical trials. *Front. Genet.* **11**, 578011 (2020).
45. Galanis, E. et al. Phase I/II trial of vorinostat combined with temozolomide and radiation therapy for newly diagnosed glioblastoma: results of Alliance N0874/ABTC 02. *Neuro Oncol.* **20**(4), 546–556 (2018).
46. Teknos, T. N. et al. A phase 1 trial of Vorinostat in combination with concurrent chemoradiation therapy in the treatment of advanced staged head and neck squamous cell carcinoma. *Invest. New Drugs* **37**(4), 702–710 (2019).
47. Puduvalli, V. K. et al. A Bayesian adaptive randomized phase II multicenter trial of bevacizumab with or without vorinostat in adults with recurrent glioblastoma. *Neuro Oncol.* **22**(10), 1505–1515 (2020).
48. Chan, E. et al. Phase I trial of vorinostat added to chemoradiation with capecitabine in pancreatic cancer. *Radiother. Oncol.* **119**(2), 312–318 (2016).
49. Paillas, S. et al. The histone deacetylase inhibitor romidepsin spares normal tissues while acting as an effective radiosensitizer in bladder tumors in vivo. *Int. J. Radiat. Oncol. Biol. Phys.* **107**(1), 212–221 (2020).
50. Livak, K. J. & Schmittgen, T. D. Analysis of relative gene expression data using real-time quantitative PCR and the 2(-Delta Delta C(T)) method. *Methods* **25**(4), 402–408 (2001).
51. Davarinejad, H., *Quantifications of Western Blots with ImageJ*. 2015.
52. Omweri, J. M. et al. Chelation chemistry of manganese-52 for PET imaging applications. *Nucl. Med. Biol.* **128–129**, 108874 (2024).
53. Pyles, J. M., Omweri, J. M. & Lapi, S. E. Natural and enriched Cr target development for production of Manganese-52. *Sci. Rep.* **13**(1), 1167 (2023).
54. Omweri, J. M. et al. PET imaging of (52)Mn labeled DOTATATE and DOTAJR11. *Sci. Rep.* **15**(1), 2395 (2025).
55. Syed, A. K. et al. Characterizing trastuzumab-induced alterations in intratumoral heterogeneity with quantitative imaging and immunohistochemistry in HER2+ breast cancer. *Neoplasia* **21**(1), 17–29 (2019).
56. Bloom, M. J. et al. Anti-HER2 induced myeloid cell alterations correspond with increasing vascular maturation in a murine model of HER2+ breast cancer. *BMC Cancer* **20**(1), 359 (2020).
57. Pukkanasut, P., et al., Voltage-gated sodium channel Na(V)1.7 inhibitors with potent anticancer activities in medullary thyroid cancer cells. *Cancers (Basel)*, 2023. **15**(10).
58. Wu, W. et al. Clinical significance of somatostatin receptor (SSTR) 2 in meningioma. *Front. Oncol.* **10**, 1633 (2020).
59. Rocheville, M. et al. Subtypes of the somatostatin receptor assemble as functional homo- and heterodimers. *J. Biol. Chem.* **275**(11), 7862–7869 (2000).
60. Klomp, M.J., et al., The effect of VPA treatment on radiolabeled DOTATATE uptake: Differences observed in vitro and in vivo. *Pharmaceutics*, 2022. **14**(1).
61. Sharma, R. et al. Upregulation of somatostatin receptor Type 2 Improves 177Lu-DOTATATE therapy in receptor-deficient pancreatic neuroendocrine tumor model. *Mol. Cancer Ther.* **22**(9), 1052–1062 (2023).
62. Xiang, X. S. et al. Histone deacetylases: A novel class of therapeutic targets for pancreatic cancer. *Biochim Biophys. Acta Rev. Cancer* **1877**(1), 188676 (2022).
63. Gillis, A. et al. Somatostatin receptor Type 2 and thyroid-stimulating hormone receptor expression in oncocytic thyroid neoplasms: Implications for prognosis and treatment. *Mod. Pathol.* **36**(12), 100332 (2023).
64. Guenter, R. et al. Overexpression of somatostatin receptor type 2 in neuroendocrine tumors for improved Ga68-DOTATATE imaging and treatment. *Surgery* **167**(1), 189–196 (2020).
65. Taelman, V. F. et al. Upregulation of key molecules for targeted imaging and therapy. *J. Nucl. Med.* **57**(11), 1805–1810 (2016).
66. Rupp, T. et al. Anti-CTLA-4 and anti-PD-1 immunotherapies repress tumor progression in preclinical breast and colon model with independent regulatory T cells response. *Transl. Oncol.* **20**, 101405 (2022).
67. Sagiv-Barfi, I. et al. Therapeutic antitumor immunity by checkpoint blockade is enhanced by ibrutinib, an inhibitor of both BTK and ITK. *Proc. Natl. Acad. Sci. USA* **112**(9), E966–E972 (2015).
68. Wu, M. et al. Converting immune cold into hot by biosynthetic functional vesicles to boost systematic antitumor immunity. *iScience* **23**(7), 101341 (2020).
69. Wang, A. et al. Somatostatin receptor 2: A potential predictive biomarker for immune checkpoint inhibitor treatment. *Pathol. Oncol. Res.* **28**, 1610196 (2022).
70. Ferone, D. et al. Somatostatin receptor distribution and function in immune system. *Dig. Liver Dis.* **36**(Suppl 1), S68-77 (2004).
71. Talme, T. et al. Somatostatin receptor (SSTR) expression and function in normal and leukaemic T-cells. Evidence for selective effects on adhesion to extracellular matrix components via SSTR2 and/or 3. *Clin. Exp. Immunol.* **125**(1), 71–9 (2001).

72. Elliott, D. E. et al. SSTR2A is the dominant somatostatin receptor subtype expressed by inflammatory cells, is widely expressed and directly regulates T cell IFN-gamma release. *Eur. J. Immunol.* **29**(8), 2454–2463 (1999).
73. Ramalingam, S. S. et al. Carboplatin and Paclitaxel in combination with either vorinostat or placebo for first-line therapy of advanced non-small-cell lung cancer. *J. Clin. Oncol.* **28**(1), 56–62 (2010).
74. Garcia-Manero, G. et al. Phase II trial of vorinostat with idarubicin and cytarabine for patients with newly diagnosed acute myelogenous leukemia or myelodysplastic syndrome. *J. Clin. Oncol.* **30**(18), 2204–2210 (2012).
75. Su, J. M. et al. Phase I/II trial of vorinostat and radiation and maintenance vorinostat in children with diffuse intrinsic pontine glioma: A Children's Oncology Group report. *Neuro Oncol.* **24**(4), 655–664 (2022).
76. Cooper, A. L. et al. In vitro and in vivo histone deacetylase inhibitor therapy with suberoylanilide hydroxamic acid (SAHA) and paclitaxel in ovarian cancer. *Gynecol. Oncol.* **104**(3), 596–601 (2007).
77. Peela, N. et al. Effect of suberoylanilide hydroxamic acid (SAHA) on breast cancer cells within a tumor-stroma microfluidic model. *Integr. Biol. (Camb)* **9**(12), 988–999 (2017).
78. Anguissola, G. et al. Kidney tubular injury induced by valproic acid: systematic literature review. *Pediatr. Nephrol.* **38**(6), 1725–1731 (2023).

Acknowledgements

Financial support is provided by the NIH NCI (R01CA240589, R01CA276540, R01CA279143), the Breast Cancer Research Foundation of Alabama, and the UAB O'Neal Comprehensive Cancer Center Preclinical Imaging Shared Facility Grant (P30CA013148). We would also like to acknowledge the UAB Cyclotron Facility and UAB Pathology Core Research Lab. The content is solely the responsibility of the authors and does not represent the official views of the National Institutes of Health.

Author contributions

S.E. Lynch, C.C., R.J.S., S.E. Lapi, and A.G.S. provided concepts, designed experiments, and supervised manuscript; S.E. Lynch and H.H. performed in vivo experiments, S.E. Lynch, C.C., P.P., J.M.O., C.G., and J.D.W contributed to in vitro assays and data analysis. S.E. Lynch performed statistical analyses and wrote the manuscript. All authors have read and approved the final version of this article.

Declaration

Competing interests

The authors declare no potential conflicts of interest.

Additional information

Supplementary Information The online version contains supplementary material available at https://doi.org/10.1038/s41598-025-94578-x.

Correspondence and requests for materials should be addressed to A.G.S.

Reprints and permissions information is available at www.nature.com/reprints.

Publisher's note Springer Nature remains neutral with regard to jurisdictional claims in published maps and institutional affiliations.